A Ground-Based Planetary Radar Array

Marc Sanchez Net*, Mark Taylor†, Victor Vilnrotter*, and T. Joseph W. Lazio‡

ABSTRACT. — This white paper describes a new ground-based planetary radar capability, implemented as an array of antennas. The motivations for ground-based planetary radar are multiple, but this white paper takes the observations of asteroids as a driving case. This choice reflects the importance of ground-based planetary radar observations in the detection, tracking, and characterization of near-Earth asteroids, which is identified as one of NASA's key roles in the National Near-Earth Object Preparedness Strategy and Action Plan. The system architecture of a planetary radar array consists of four major subsystems—the array element, of which the antenna is a major component; the signal processing; array services and infrastructure; and operations computing and software. Each of these major subsystems is described briefly, with references to previous implementations or analog systems. A life-cycle cost model is presented, which includes a contribution from the operations cost. This life-cycle cost model has multiple parameters, including antenna diameter, the transmit power at each antenna, and the number of antennas. We perform a tradespace exploration to find optimal design points, with a design goal of meeting the previous capability of the Arecibo Observatory's planetary radar. A strength of this architecture is that it is scalable, so that improved capabilities could be realized.

I. Introduction

Ground-based radar observations have been used to probe the surfaces of all of the planets with solid surfaces and many smaller bodies in the solar system [1]. Notable findings include characterizing the distribution of water at the south pole of the Moon [2, 3], the first indications of water ice in the permanently shadowed regions at the

*Communications Architectures and Research Section.

†Communications Ground Systems.

‡The Interplanetary Network Directorate.

The research described in this publication was carried out by the Jet Propulsion Laboratory, California Institute of Technology, under a contract with the National Aeronautics and Space Administration. © 2022. California Institute of Technology. Government sponsorship acknowledged.

poles of Mercury [4, 5], polar ice and anomalous surface features on Mars [6], establishing the icy nature of the Jovian satellites [7], and the initial characterizations of Titan's surface [8].

More recently, there has been considerable interest in using radar observations to characterize near-Earth asteroids (NEAs) and determine their orbits precisely. The motivation for radar observations of asteroids is threefold. First, asteroids represent primitive remnants of the early solar system, and characterization of their properties can provide insight into their evolution and parent population(s) [9]; second, they represent targets for exploration by spacecraft (e.g., [10]), both robotic and crewed; and third, precise knowledge of their orbits, shapes, sizes, and bulk densities is essential to assess the extent to which they might represent impact hazards to Earth [11]. As described in the National Near-Earth Object Preparedness Strategy and Action Plan, ground-based planetary radar observations are an integral element of enhancing the detection, tracking, and characterization of NEAs. In this respect, [12–16] have presented analyses of the performance of ground-based planetary radars (Arecibo Observatory [AO] and the Goldstone Solar System Radar [GSSR]). Among their conclusions is that ground-based planetary radars can reduce orbit uncertainties by as much as a factor of 10^5, with the potential benefit of extending the duration over which impact hazard assessment can be made by a factor of five (from decades to centuries).

Finally, in addition to providing direct science measurements, the ground-based planetary radar infrastructure has assisted in the recovery of spacecraft. The most notable example was determining the Solar and Heliospheric Observatory (SOHO) spacecraft attitude, thereby allowing the recovery of the mission, which continues operation to this day [17]. A more recent example is the recovery of the lunar-orbiting (but defunct) Chandrayaan-1 spacecraft, which had been thought to have crashed into the surface of the Moon [18, 19].

The rest of this article is organized as follows: First, we discuss the motivation for a planetary array system and emphasize the need to replace the capabilities lost by the demise of Arecibo. Specifically, we lay out the goal of replacing at least the capability of Arecibo and the desire for a much improved capability (factors of several to 10). In order to achieve this goal, this white paper describes the architecture of a planetary radar system based on an array of ground antennas. These antennas, while individually smaller in diameter than the 305-m Arecibo dish, use signal processing to coherently combine the transmitted and received signals, thus achieving a larger effective aperture and higher sensitivity than Arecibo. We discuss the architecture of a monostatic planetary radar system, including the performance and cost models used for high-level tradespace exploration. Finally, we apply these models to provide recommendations on the next-generation planetary radar system.

II. Motivation

The planetary radar infrastructure (Figure 1), prior to the collapse of Arecibo, was capable of observing all terrestrial planets, the larger main-belt asteroids, the largest moons of Jupiter and Saturn, and NEAs at distances of order 0.1 au, with typical NEAs being several hundred meters in diameter (Figure 2). Smaller NEAs could be observed at smaller distances, with objects of order 10 m and smaller having been observed at distances less than 1 lunar distance. With its high gain and large transmit power, the AO was able to detect targets at the largest distances. However, the AO had a limited declination range and was able to observe only approximately 30% of the sky (centered approximately on a declination of 18°). By contrast, the GSSR, either monostatically or bistatically with the Green Bank Telescope (GBT), can observe approximately 75% of the sky. Reference [16] provides further technical details and comparisons between the various facilities.

With the collapse of the AO on December 1, 2020, the scientific community lost an invaluable asset for planetary radar science and planetary defense. The motivations for enhancing the current radar infrastructure are varied, including

- This loss occurred approximately three years before the start of the Legacy Survey of Space and Time (LSST) to be conducted at the Vera C. Rubin Observatory, which is projected to provide a substantial increase in the number of NEAs, including potentially hazardous ones (e.g., [20, 21]); the Near-Earth Object Surveyor space telescope (NEO Surveyor, née NEOCam) has also been

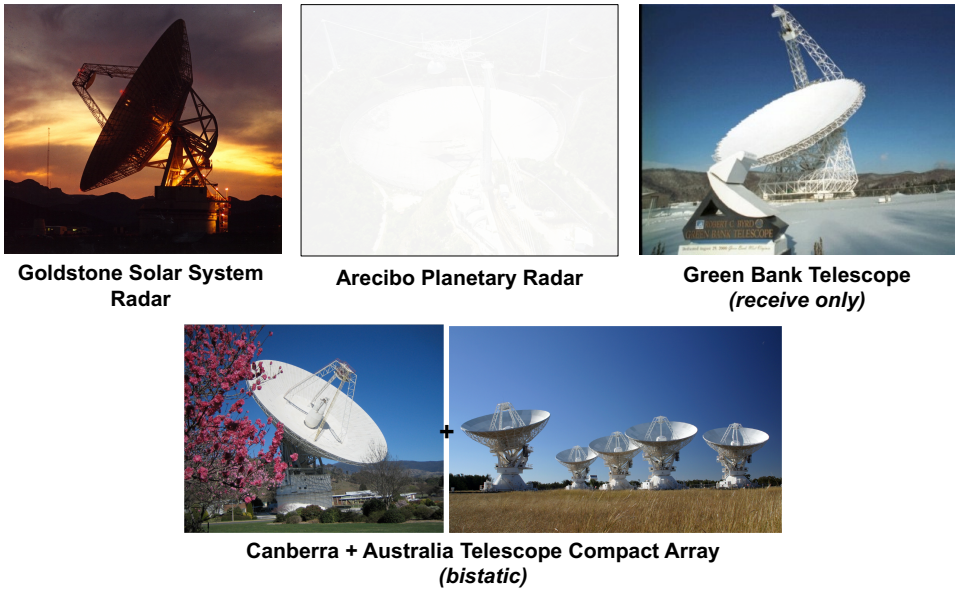

Figure 1. The international planetary radar infrastructure has enabled a variety of discoveries about all terrestrial planets, the largest moons, and NEAs. (Arecibo is shown in gray to indicate that it is no longer functional.)

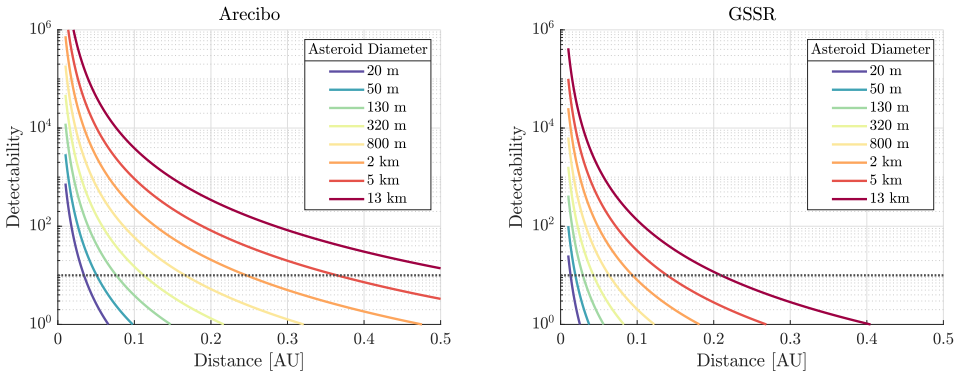

Figure 2. Left: Detectability of an asteroid as a function of its diameter using the AO in monostatic mode and operating at 2380 MHz (S band). The asteroid is assumed to have an albedo of 0.18 and rotate at a rate of 2 h per revolution. The black dotted line indicates a detectability level of 10 dB, which has been shown to result in reliable asteroid detection in the past. Right: Detectability of an asteroid as a function of its diameter using the GSSR in monostatic mode and operating at 8560 MHz (X band) with the same asteroid assumptions.

approved to enter Phase B, and it is explicitly designed to find potentially hazardous asteroids.

- "Minimoons," asteroids captured into metastable orbits around the Earth, are another class of objects for which there is growing interest, both from a scientific perspective and because they could be easily accessible targets for technical demonstration missions [22]. The number of detected minimoons is likely to increase concomitantly with the increase in NEAs.

- With the potential increase in spacecraft in the cislunar environment, both government and commercial, ground-based planetary radar observations could be an integral aspect of safety and mission assurance (SMA). Analogous to the GSSR recovery of Chandrayaan-1, a planetary radar could be used to track spacecraft, either cooperative or noncooperative. In other contexts, this activity is often termed "space domain awareness" (SDA).

- The technical infrastructure that led to the suite of planetary radar discoveries summarized above—namely single large radio antennas equipped with vacuum tube (klystron) microwave amplifiers—has not changed substantially in the past half-century. The Deep Space Station 14 70-m antenna on which the GSSR is installed is nearing 60 years of operational use, as was Arecibo prior to its collapse.

This set of considerations motivates the goal of at least replacing the Arecibo capability and, ideally, expanding beyond it.

III. System Architecture

In this section, we present the high-level architecture of a ground-based planetary radar based on an array of antennas. Figure 3 presents a functional decomposition of the system that includes four main subsystems: the array of antennas, the synchronization electronics, the signal processing systems required to transmit the radar waveform and receive the asteroid echoes, and the control and computing software necessary for operating the array. The focus of this white paper is primarily on the physical infrastructure of a planetary radar array, illustrated by application to a specific use case (§V). The concept of operations, on the other hand, is less a focus of this white paper. However, implementation of the planetary radar array would allow the operations concept to be further specified and, ultimately, to assess whether greater efficiencies or more remote operations could be introduced than has been traditional with either Arecibo or the GSSR.

For the vast majority of planetary radar observations, the target is not angularly resolved, i.e., its apparent angular size is (or has been) less than the angular resolution of the receiving antenna. The target detectability is approximately equal to

$$D = \frac{P_{rx}}{P_n}\sqrt{\Delta T \Delta f}, \tag{1}$$

where P_{rx} and P_n denote the echo and noise power received at the antenna, and $\Delta T \Delta f$ is the bandwidth-time product for the observations (Figure 2).

The received power is determined by the radar equation

$$P_{rx} = \frac{\lambda^2}{4\pi} P_{tx} G_{tx} G_{rx} \frac{\sigma}{(4\pi)^2 R^4}, \tag{2}$$

where G_{rx} is the antenna gain of the receiving antenna, G_{tx} is the antenna gain of the transmitting antenna, P_{tx} is the power transmitted by the transmitting antenna, λ is the wavelength of observation, σ is the radar albedo or the radar cross-section, and R is the range or distance to the target.[1] The notable factor of R^{-4} in the radar equation can be considered to be the consequence of Huygens' Principle—the transmitted signal suffers an R^{-2} loss by the inverse-square law while travelling to the target; the illuminated surface of the target then reradiates this signal, which suffers an additional factor of R^{-2} loss upon its return to the receiving antenna.

Obtaining sufficient signal-to-noise ratios requires large values of G_{rx}, G_{tx}, and P_{tx} in order to compensate for the R^{-4} factor. Traditionally, this requirement has been satisfied by building large monolithic antennas. For instance, in the mid-1960s, both

[1] This "classical" form of the radar equation assumes that the range or distance to the target from both the transmitting and receiving antennas is approximately the same. There have also been bistatic radar observations in which the transmitter or receiver was located on a spacecraft in the vicinity of the target body. In such a scenario, the R^{-4} factor can be replaced by approximately R^{-2}. While we do not consider such bistatic radar scenarios in this white paper, a radar array also benefits such observations.

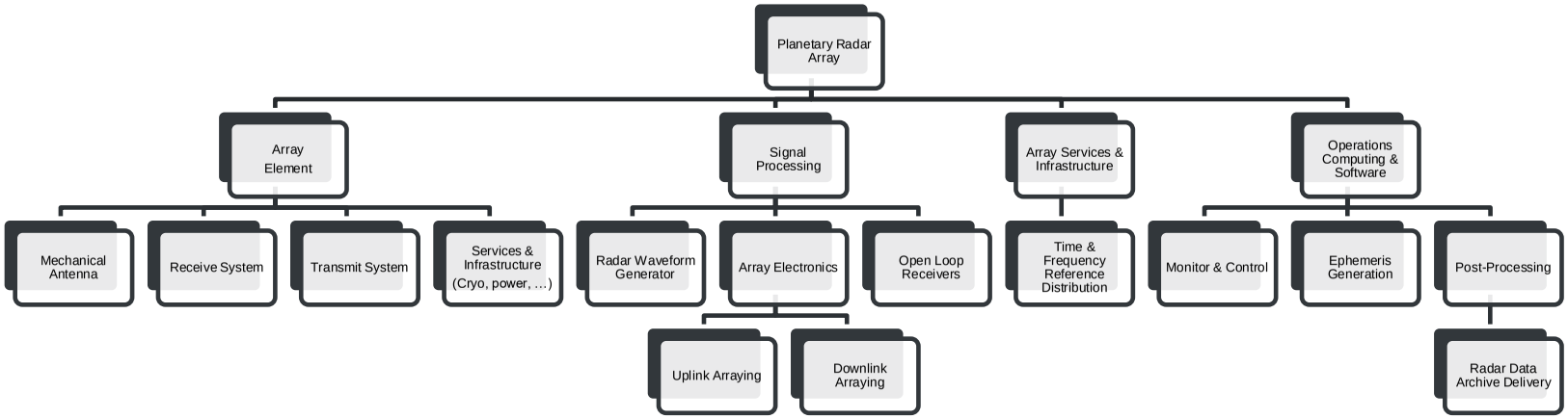

Figure 3. System architecture of a ground-based planetary radar array.

the 305-m parabolic reflector of Arecibo and the three 64-m antennas, later upgraded to 70-m diameters, of the Deep Space Network (DSN) were constructed; the GBT provides a 100-m parabolic dish. At the time, this architecture was reasonable, but the steadily decreasing cost of electronics has led to an array architecture increasingly being adopted. The concept of an antenna array is simple: Combine the signal transmitted and/or received by a collection of "small" antennas in such a way that the total system performance is equal to that of a much larger monolithic antenna. It does require careful design and implementation of the signal processing and electronics components to achieve the theoretical arraying gain, but it is now the standard approach for (receive-only) radio astronomy telescopes.

Several reasons motivate our choice of a planetary radar system based on an array of ground antennas: First, large monolithic antennas are expensive to build, operate, and maintain, especially when large sky coverage is required. In that sense, several independent studies conducted at the Jet Propulsion Laboratory (JPL) and elsewhere have evaluated the trade between antenna diameter and number of arrayed antennas. They have consistently found that even if technically feasible, large monolithic antennas have a significantly higher life-cycle cost than arrays of smaller antennas [23–27], a finding further vindicated by investments in arraying technology by the DSN and other ground-based science observatories (e.g., the Very Large Array [VLA], the Australian Square Kilometre Array Pathfinder [ASKAP], the Karoo Array Telescope [MeerKAT]); it is also notable that, with the possible exception of the Qitai Radio Telescope (QTT), no *fully-steerable* radio telescopes have been constructed or even planned since the completion of the construction of the GBT in 2000. Second, arrays of antennas offer significant advantages in terms of capability degradation due to the planned or unplanned maintenance. Indeed, when a large monolithic antenna needs to be serviced, the entire system capability is temporarily lost. In contrast, an array of antennas simply experiences a temporary service degradation, which can be shown to be increasingly small as the number array elements increases.

Finally, because an antenna array is specified using three degrees of freedom, the gain and transmit power of each element, as well as the number of elements in the array, it can be designed to optimize both sensitivity and sky coverage. As an example, consider the case of two monolithic systems such as the AO and the GSSR: While the former was 15 times more sensitive than the latter, it could only survey 32% of the accessible sky compared to 79% for the GSSR [16]. An array of ground antennas can be designed to achieve the sensitivity of the AO as well as the sky coverage of the GSSR.

A. Array Element

In this paper, we consider a planetary radar array in which each array element is implemented using a mechanically-steered parabolic antenna connected to a transmit and a receive subsystem. Each element is complemented by infrastructure to support

its operations.

1. Mechanical Antenna

The mechanical antenna includes all stationary and moving parts of the primary reflector and subreflector, its control mechanisms (both in azimuth and elevation), the pedestal, and its foundation. Its design is primarily driven by two factors: the size of the dish and the location of the high-power amplifier.

The size of the antenna determines which technologies are available for manufacturing the main reflector and its supporting mount. For smaller antennas, on the order of 10 m or less, hydroforming has been shown to be a cost-efficient option for mass production. With this technology, the reflector significantly contributes to the required structural rigidity of the antenna and prevents coherent radiation from leaking between adjacent antennas in the array [28]. However, as the diameter of the antenna increases, the exact shape of the hydroformed reflector becomes increasingly hard to control and, consequently, the illumination efficiency of the reflector decreases.

Panelized antennas have been demonstrated in several operational systems including the DSN 70-m and 34-m subnetworks, the European Space Agency's Estrack stations, the Japanese Aerospace Exploration Agency's (JAXA) Usuda and Misasa antennas, and the VLA, among others. They are assembled from a collection of panels that are first individually manufactured and then mounted on a truss structure that can be fined-tuned to achieve excellent illumination efficiency even when operating at high frequency bands (30 GHz or higher). Furthermore, they are typically coupled with gear-driven mounts to allow the reflector and subreflector to rotate both in azimuth and elevation, thus providing excellent sky coverage.

Each antenna is coupled with a high-power amplifier, which can be placed either on the structure in a typical antenna (Figure 4, left) or on the ground in the case of a beam-waveguide (BWG) antenna (Figure 4, right). In the latter case, radio frequency (RF) power is transmitted out the antenna through a series of RF mirrors and then to the subreflector/main reflector. BWG antennas are used by the DSN, at the JAXA ground stations, and at the Sardinia Radio Telescope/Sardinia Deep Space Antenna, and have been shown to result in improved system operability and maintenance without compromising system performance.

2. Transmit System

For over a century, vacuum tube amplifiers have served as the standard source for high-power RF signals used in communications and radar transmitter systems. Specifically, klystron tubes are typically used for applications from the ultra-high frequency (UHF) up to around 200 GHz (Figure 5). Within this frequency range and for relatively narrowband applications, klystrons are unparalleled in their RF output power capability, gain, and efficiency. Klystron tubes can output, depending on

Figure 4. Examples of mechanical antennas that could be candidates for use in a planetary radar array. Left: Illustration of an 18-m next-generation Very Large Array (ngVLA), which has an offset feed design (mtex/NRAO/AUI/NSF). Right: DSN 34-m BWG antenna. These operate to frequencies of at least 32 GHz; are used routinely for spacecraft tracking, telemetry, and command; and have been demonstrated as a transmit uplink array for sending commands to spacecraft and have been arrayed for planetary radar observations.

frequency, anywhere from kilowatts to hundreds of kilowatts, and can be arrayed to produce megawatts of continuous-wave RF output power. Additionally, 60 dB of amplifier gain is not uncommon. The GSSR employs two 250-kW klystrons operating at 8560 MHz, and Arecibo employed two 500-kW klystrons operating at 2380 MHz. Despite their tremendous power advantage over other technologies, their implementation presents challenges.

One such challenge is the often limited lifetime and reliability for these devices, particularly when operating at very high power levels and for applications that involve pulsed modulation schemes resulting in significant thermal cycling. Klystrons amplify a small input signal using a high-density electron beam. Beam formation requires the use of a high-potential electron gun, and this high-voltage requirement adds size and complexity to the transmitter and associated power supply. Additionally, typical klystron efficiency does not exceed 50%. When coupled with the large power densities within the electron beam, localized heating tends to limit lifetime and reliability for the high-power klystrons, particularly at higher frequencies.

Other challenges arise from the complex nature of the devices. Klystrons must be custom designed for a given frequency of operation and typically require specialized tuning once they are assembled. Consequently, large-scale and timely manufacturability can be difficult. There are only a handful of vendors worldwide with the capability and infrastructure to develop these devices. New designs can take months to years to refine, and costs for a new design can range from hundreds of thousands to a few million dollars. Klystron failures are typically catastrophic, requiring immediate replacement by a spare in order to prevent significant transmitter downtimes. If repair is possible, repair times typically take several months and costs are usually a significant portion of the cost for a new klystron.

Though vacuum tube amplifiers are not likely to disappear anytime soon, recent advances in solid-state amplifier technology is providing a potential alternative to the

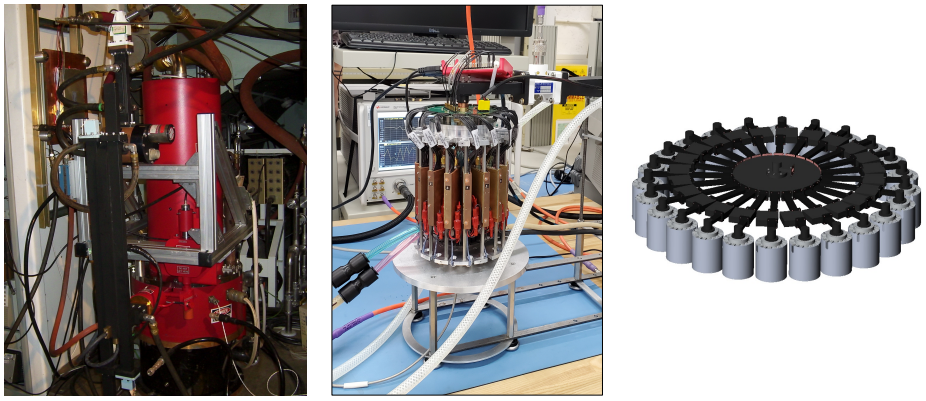

Figure 5. Left: Klystron (high-power microwave amplifier) that provides 80 kW of output power at a frequency near 7.1 GHz and is used for spacecraft telemetry, tracking, and communications within the DSN. For reference, the unit stands approximately 1.2 m tall. Middle: Prototype solid-state microwave amplifier that has been developed at JPL. This unit produces 1.1 kW of output power at frequencies near 8.56 GHz. This solid-state module consists of 16 solid-state 80-W monolithic microwave integrated circuit (MMIC) amplifiers, which are visible as the vertical boards. The outputs of the 16 amplifiers are combined coherently to produce the 1.1 kW of output power through the waveguide at the top of the unit. For reference, this prototype unit is approximately 0.2 m tall. Right: Design of a 25-kW amplifier system composed of multiple solid-state units shown in the middle panel. This design (2-m diameter) uses radial combining and illustrates how the use of solid-state units enables a modular architecture.

use of vacuum tubes for high-power transmitter systems (Figure 5). While individual solid-state transistors are orders of magnitude lower in output power compared to tube amplifiers, techniques for combining many of these devices in parallel could potentially achieve comparable output power and efficiencies. Solid-state transmitter systems are a burgeoning technology that has been steadily maturing over the past two decades. Solid-state transmitter systems have been implemented extensively in radar and communications systems across multiple industries such as civilian and military aircraft, telecommunications including wireless/cell phone technology (5G), and spacecraft.

Solid state–based transmitter systems provide some advantages over tube-based systems. The lifetime and reliability of solid-state devices is a vast improvement over certain types of tube amplifiers, such as klystrons. Additionally, the modular nature of solid-state power amplifiers (SSPAs) and large number of elements in parallel allow for the design of robust transmitters that exhibit graceful degradation as opposed to catastrophic failure. Both of these aspects together provide for a reduction of transmitter maintenance time and costs. Also, solid-state devices are generally low-voltage devices that do not require high-voltage infrastructure and power supplies, which are considerably larger and require significant safety considerations such as arch mitigation. Solid-state transmitter technology comes with its own challenges, however. For instance, low voltage in this case corresponds to high current and requires a high-current infrastructure relatively close to the source to mitigate resistive heating and voltage losses in the direct-current (DC) path. Additionally, the technology is relatively new in comparison to tube amplifiers, and development efforts to improve

efficiency, combining techniques, power output, scaling, higher frequency, and costs are ongoing.

The elemental and modular nature of SSPAs lends well to newly developing radar techniques such as antenna and panel-style active phased array transmitting. Antenna arrays consist of a network of smaller, lower-power antennas, each with an individual coherently synced transmitter. Active phased array panels use multiple closely spaced (typically every $\lambda/2$, but other spacing is used depending on the application) low-power antenna elements that coherently combine into a single signal in free space. These arrays naturally take advantage of the compact size, large-scale manufacturability, scalability, and electronic controllability of parallel individual SSPA elements, as well as the reduced maintenance cost and simplified infrastructure associated with solid-state transmitters. The concurrent development of SSPA technology alongside transmit array technology is complementary, and it is foreseeable that solid-state transmitter systems will play a significant role in the next-generation planetary radar assets over the coming decades.

3. Receive System

In the architecture considered here, the individual antennas of a planetary radar array would be outfitted with receivers as well as transmitters.[2] These receivers would allow the array to function in a monostatic mode, receiving signals that it transmits, or bistatic mode, receiving the signals from other (planetary radar) transmitters. Such receivers are a well-developed technology and would be based on similar systems from radio astronomy and the DSN (e.g., [29–31]). An architecture in which different antennas are used for transmit and receive is also possible, but it is not considered here because of largely programmatic concerns (e.g., oversight of potentially two antenna vendors and potentially larger land acquisition costs).

Specifically, existing radio astronomy and DSN receiving systems cover frequencies from 2 GHz to 40 GHz, are equipped with cryogenic receivers that operate at extremely low equivalent noise temperatures (e.g., 18 K at X-band at the DSN), and can have octave bandwidths. These characteristics are sufficient for use in a planetary radar array, and the primary factor that would require attention would be the optics of the antenna to ensure that the receiver is well illuminated by the antenna and that both same-sense and opposite-sense polarizations can be collected simultaneously.

4. Services and Infrastructure

Each array element will require a common set of infrastructure services to operate. These include, for instance, distribution of power (excluding the high-power amplifiers,

[2] An alternative implementation in which only a subset of antennas are equipped with transmitters is also possible. This takes advantage of the fact that in transmit mode, the performance of an array of antennas scales as N^2, whereas in receive mode it only scales as N.

which have their own power generators); water; liquid nitrogen for cryocooling, heating, ventilation, and air conditioning (HVAC); and TV feeds for surveillance. Additionally, each element of the array will require construction of roads to access the mechanical antenna and its supporting equipment, as well as trenches for laying out underground cables to connect the antenna with the array's operations center.

B. Synchronization

The planetary radar will require several systems to ensure that all elements in the array remain synchronized (in time) and syntonized (in frequency). Synchronization and syntonization are particularly important when designing and operating an uplink array because the theoretical gains of the array only materialize when the electric fields radiated by each antenna, in the far field, add coherently in phase.

Because uplink arraying has successfully been demonstrated by the DSN with up to three antennas (e.g., [32]), the equipment necessary for proper synchronization and syntonization is well developed. In particular, hydrogen masers have been employed as the primary DSN frequency standard for several years and provide frequency offsets relative to Coordinated Universal Time (UTC) of less than 3×10^{-13}. This reference can be used to drive oscillators at intermediate and carrier frequencies, generate ultra-stable 1-PPS (pulse per second) signals, and drive master clocks that provide ultra-precise time references across the array.

In order to achieve this level of precision, the planetary radar system will house all equipment to generate time and frequency references in a centralized location, within an environmentally controlled area. These references will then be distributed to each array element using an underground network of cables. Methods to calibrate changes in the cable length (and thus time delay) due to thermal and other environmental factors have been developed and allow for a resolution of less than 10 ps, which is sufficient for uplink arraying purposes and was demonstrated with continuous-phase monitoring [33]. However, the ability to maintain this level of precision over radar tracks spanning several hours is yet to be demonstrated.

C. Signal Processing

1. Radar Waveform Generator

Several radar waveforms are used currently for planetary radar investigations. This is due to several considerations: First, targets can be either underspread or overspread, depending on their size, range, and spin rate [34]; second, the radar needs to be operated under varying degrees of uncertainty in the ephemeris, shape, and dynamics of the body being observed.

In the architecture described here, each array element will be equipped with a radar waveform generator supporting at least three modes of operation: Continuous Wave

(CW), Binary Phase-Coded (BPC), and Linear Frequency Modulation (LFM or "chirp"). These modes are already operational in the GSSR and, therefore, the technology required to implement them is well understood [35].

In CW mode, the radar transmits an unmodulated tone and receives its echo in the same-sense and opposite-sense polarization. The measured signal provides information about the radar cross-section, surface roughness, and rotational state of the target but does not allow for mapping the asteroid surface [35, 36].

The BPC and LFM modes are two well-known pulse-compression techniques that expand the capabilities of the CW mode by providing time discrimination properties to the received signal. This allows the radar to perform range measurements, refine ephemeris of the target asteroid, and calculate delay-Doppler maps (DDMs), which can then be translated into the target's natural coordinates to obtain images of its surface [34]. The key performance characteristics of the BPC and LFM modes are the pulse repetition frequency and the chip duration. The former determines properties such as maximum measurable Doppler shift and unambiguous range, while the latter is proportional to the radar's spatial resolution. In practice, therefore, we expect the planetary radar to provide a wide range of configuration settings so that its operation can be optimized depending on the target of interest. As an example, the GSSR currently supports several chip rates and pulse repetition frequencies, allowing researchers to select resolutions ranging from 1 km to less than 10 m.

For overspread targets such as Mars, Europa, or Ganymede, DDMs cannot be estimated using the standard BPC mode. Instead, "long-code" methods have been developed and used operationally at Arecibo [34], as well as tested at the GSSR. Such "long-code" methods would also be able for the proposed planetary radar system.

2. Uplink Array Electronics

In order to achieve coherent uplink arraying, the planetary radar will require a suite of systems to calibrate the transmitted electric fields and ensure coherence in the far field. To this end, the radar system will be equipped with the following subsystems:

- Antenna pointing predicts: Using known ephemerides from the target, this subsystem will calculate azimuth and elevation profiles of each antenna in the array, over time, and deliver them to the respective antenna control systems. These calculations will be performed offline prior to each radar track.
- Antenna Doppler pre-compensation: Using known ephemerides from all antennas in the planetary radar, this subsystem will calculate relative Doppler shifts between each element in the array (due to different latitude and longitude coordinates on Earth) and deliver them to the respective radar waveform generators. These calculations will be performed offline prior to each track.
- Antenna delay pre-compensation: This subsystem will estimate differences in

time-delay between the different elements in the array to ensure that all radar waveform generators transmit synchronously. These estimates and any required corrections will be initially calibrated prior to the start of each radar track and will be adjusted periodically for long duration tracks (tens of minutes or longer).

- Uplink array calibration: Using ephemerides for a known target (e.g., Tycho Crater on the Moon [37]), the calibration subsystem will ensure that the phase of the electric fields transmitted by each array element is properly synchronized to achieve coherent interference at the target. This calibration will be performed at the beginning of each radar track, after Doppler and delay pre-compensation. Once successful calibration has been established, the planetary radar will rotate all participating antennas to the desired target and the actual science investigation will commence.

D. Downlink Array Electronics

The use of arrays for radio astronomical observations has been standard for decades, and the 1974 Nobel Prize in Physics was awarded in part for the development of techniques related to arrays of antennas. Today, radio astronomical arrays with tens of antennas are operated routinely (e.g., 27-antenna VLA, 30-antenna Giant Metrewave Radio Telescope, 36-antenna ASKAP, 64-antenna MeerKAT), and arrays with hundreds of antennas are being designed (Phase 1 of the intermediate frequency Square Kilometre Array [SKA1-Mid]). In the context of the DSN, downlink arraying has been used in operations for several decades. For instance, the first full-spectrum arraying system was developed and successfully deployed in 1996 to support the Galileo mission[3] [38]. Since then, the DSN has improved its arraying capabilities, and today allows for full-spectrum combining of two, three, or four 34-m antennas, as well as arraying of 34-m and the 70-m antennas [31].

For the planetary radar array, the system would be outfitted with electronics capable of full-spectrum combining (FSC). In particular, each array element will down-convert the received RF signal into an intermediate frequency (IF) and deliver it to the FSC receiver, which will digitally sample all inputs simultaneously. Coherent combining of these samples will be achieved using an FSC combiner, and the resulting output will be up-converted to the original IF frequency so that, from the point of view of science processing, there is no difference between the output of a single antenna and the array [38].

Finally, because simultaneous dual polarization measurements are necessary for planetary radar investigations, two parallel downlink array electronics will need to be built and operated concurrently, one per polarization.

---

[3] Arraying in the context of interplanetary communications was demonstrated as early as 1986 when Voyager 2 flew by Uranus. However, the arraying technique was not full-spectrum combining, which has since become popular for deep space communications and other radio science activities.

1. Open Loop Receivers

Open Loop Receivers (OLRs) are currently used at the DSN for radio science investigations, Delta-Differential One-way Ranging (DDOR) measurements, and other science activities. We expect that the planetary radar system would utilize similar OLRs to capture in-phase and quadrature (I/Q) samples of the received echoes.

Several OLRs will be available in the planetary radar system, allowing users to sample the received signal for each individual array element, as well as collect I/Q samples of the combined signal generated by the FSC combiners (in both polarizations). Each OLR will allow the operator to record I/Q samples over a user-defined range of frequencies. To achieve this goal, it will down-convert the received IF signal via a local oscillator using a predefined and possibly time-varying frequency offset, which will be precomputed ahead of each radar track depending on the asteroid ephemeris and the geometry of the radar track. Additionally, each OLR will be able to operate over a wide range of bandwidths, from a few hertz to several megahertz, and different sample resolutions (bits per sample). This will ensure that recordings can be captured regardless of the mode of operation and uncertainty in the asteroid ephemeris.

E. Operations Computing and Software

The planetary radar array will be operated centrally using a suite of monitor and control software that includes all necessary functionality to schedule tracks in the array, compute the necessary information to conduct the science tracks (e.g., ephemeris propagation), monitor the state of the system while in operation, detect and report any anomalies, and perform common post-processing activities. Additionally, the system will provide the required interfaces for long-term archival of the observations.

F. Calibration

A critical element of a radar array is that it be phased, i.e., the electric fields from the individual antennas must add coherently in the far field of the array. Meeting this requirement has two elements: (i) The delays to each antenna must be measured and any temporal changes (e.g., due to changing temperatures producing different electrical paths) must be monitored and compensated; and (ii) the relative velocities between the antennas must be removed, necessitating an ephemeris for the target.

Techniques for calibrating the delays for a (receive-only) radio astronomical array using a *reference emitter* are mature for radio astronomical (receive-only) arrays. In principle, for a radar array round-trip phase measurements could be conducted to monitor the delays to each antenna. However, it is generally difficult to measure the phase contributed by the feed or the horn at the antenna, and the lines of sight from the different antennas through Earth's atmosphere can have differential delays.

Because the radar waveforms are relatively narrow band, and CW transmissions are

by definition, the compensation of the relative velocities is comparable to the Doppler shift compensation conducted during spectral line observations for radio astronomical Very Long Baseline Interferometry (VLBI).

Crucially, for a transmitting array, these considerations have led to the concept of a *reference receiver*. Different scenarios have been developed and initial tests conducted to verify the approaches [33, 39]. These different approaches consist of a distant receiver or using the Moon as a target (Figure 6); for a future operational system, a receiver in geosynchronous orbit (GEO) has been proposed.

Figure 6. Two arrays of antennas that have been used to demonstrate aspects of arraying for planetary radar. Left: Loop Canyon uplink array of five 1.2-m antennas. Among the demonstrations that this system conducted was preliminary phasing of a five-element array of small (1.2-m) antennas using a nearby signal source on the ground as reference [40]. Right: DSN 34-m antennas at Apollo Valley, configured as a three-element interplanetary Uplink Array. Among the demonstrations conducted with this system include two-element array gain via the Mars-orbiting spacecraft Mars Global Surveyor (MGS) [41], and two- and three-element array gain and phase stability measurements with the EPOXI spacecraft [33].

.

Phased arrays are, of course, standard for terrestrial radar applications, and there have been limited DSN experiments of phasing transmit antennas (the DSN "Uplink Array" and the Loop Canyon Array, e.g., [42–44]). These experiments demonstrated the expected N^2 improvements for coherent addition of antennas, but they were not required to demonstrate the range (distance) and range-rate (Doppler) precision required for ground-based planetary radar. Additional work is necessary to verify that the required precision can be obtained.

IV. Tradespace Exploration

A. Performance Model

To evaluate the performance of a planetary radar system, we focus primarily on estimating how far away from Earth a target could be detected given basic characteristics such as size, radar albedo, and rotational period. Therefore, instead of studying the performance of the system with respect to the signal-to-noise ratio of the

received I/Q samples, we use detectability as our figure of merit. This approach matches previous work in the literature, but we extend the formulation here to account for the fact that radar is composed of an array of antennas [16, 45].

To simplify the problem, we assume that the radar operates in BPC mode and the target is underspread or moderately overspread so that long-code techniques need not be used. We also consider that an asteroid is detectable if the amount of echo power in a given cell of the measured delay-Doppler cell exceeds the root-mean-square statistical fluctuation of the receiver's thermal noise by a certain threshold. We relate detectability and signal-to-noise ratio by [34]

$$D = \sqrt{\Delta T \Delta f} \cdot \mathrm{S/N}, \tag{3}$$

where ΔT is the total integration time, Δf is the required frequency resolution, and S/N denotes the signal-to-noise ratio of each cell in the delay-Doppler image. Additional figures of merit such as range resolution or range and frequency ambiguity could also be considered, but we assume here that the waveform radar generator provides a wide enough set of configuration parameters to properly configure the radar for each specific target. Further, in monostatic operation, ΔT is at most equal to half of the radar track duration because the radar antenna must switch between transmit and receive.

1. Signal-to-Noise Ratio

The received power echo P_{rx} can be estimated using the monostatic radar equation

$$P_{rx} = \frac{P_{tx} G_{tx} G_{rx} \lambda^2 \sigma}{(4\pi)^3 R^4}, \tag{4}$$

where P_{tx} denotes the transmit power, G_{tx} and G_{rx} denote the transmit and receive gain, λ is the carrier wavelength, σ is the radar cross-section or radar albedo, and R denotes the distance between Earth and the object being studied. An analogous equation can also be found for the case of a bistatic radar system, a consideration not considered here for simplicity's sake.

Basic manipulation of Equation (4) yields

$$P_{rx} = \frac{1}{4\pi\lambda^2} P_{tx} A_e^2 \frac{\sigma^2}{R^4}, \tag{5}$$

where A_e is the effective area of the planetary radar system and we have once again assumed monostatic operation so that the transmit and receive gains are equal.

2. Noise Power

We assume that the OLRs collect I/Q samples at a rate of f_s samples per second. We also assume that the antennas of the planetary radar system have an equivalent noise system temperature T_{sys} that is approximately constant for the duration of the

observation track (i.e., during ΔT seconds). The noise power of the individual I/Q samples is then

$$P_{\text{IQ}} = kT_{\text{sys}} f_s, \tag{6}$$

where k denotes the Boltzmann constant.

The samples collected for the echo of a given pulse are processed using a discrete Fourier transform (DFT) to obtain DDMs of the target asteroid. The DFT is known to be equivalent to a coherent integrator from the point of view of noise and acts as a filter for each DFT bin. Therefore, the noise power after DFT processing is approximately equal to

$$P_n = kT_{\text{sys}} \Delta f, \tag{7}$$

where Δf is the frequency resolution of the DFT which is, by definition, equal to the value used in Equation (3). Therefore, the target S/N ratio is equal to

$$\text{S/N} = \frac{P_{rx}}{P_n} \tag{8}$$

3. Target Characteristics

The radar cross-section of an asteroid can be approximately expressed as the product of its albedo (or reflectivity) and the projected area in the radial direction. For instance, and assuming an approximately spherical asteroid,

$$\sigma = \alpha \pi \frac{S^2}{4}, \tag{9}$$

where α denotes the asteroid's albedo and S denotes its average diameter. Additionally, the reflected power from an asteroid will have frequency components over a bandwidth dictated by its rate of rotation. In particular, [45] shows that for an approximately circular asteroid, the bandwidth of the echo reflection can be upper-bounded by

$$B \leq \frac{4\pi S}{\lambda P}, \tag{10}$$

where λ and S are defined as before, and P is the period of rotation of the asteroid.

4. Target Detectability

Combining Equations (3), (9), and (7) provides a single equation that relates the ability to detect an asteroid with basic system parameters:

$$D = \frac{1}{4\pi\lambda^2 k} P_{tx} \frac{A_e^2}{T_{\text{sys}}} \frac{\sigma}{R^4} \sqrt{\frac{\Delta t}{B}}. \tag{11}$$

This expression agrees with previously derived results by [45] and [16]. However, a more formal derivation by [34] shows that a correction factor of 2/3 is needed to

account for the nonideal properties of a rectangular pulse ambiguity function, which translates to a 1.76-dB loss with respect to the ideal case.

Next, we specialize Equation (11) for the case of an array of antennas. In particular, let N denote the number of antennas in the array, and let D_a and P_a indicate the diameter and transmit power of each array element, respectively. Then, an asteroid's detectability is equal to

$$D = \underbrace{\frac{\pi\eta}{4^3\lambda^2 k T_{\text{sys}}}}_{\text{constant}} \cdot \underbrace{N^3 P_a D_a^4}_{\text{system factor}} \cdot \underbrace{\frac{\sigma}{R^4}\sqrt{\frac{\Delta t}{B}}}_{\text{target factor}}. \tag{12}$$

In this formulation, we have assumed the receiver noise temperature T_{sys} to be a constant. Similarly, we have used η to denote the overall array efficiency, which is equal to

$$\eta = \eta_{arr} \cdot \eta_{ant}^2 \cdot \eta_{ddm}, \tag{13}$$

where η_{arr} is the arraying efficiency and captures system performance loss due to the inability to achieve perfect uplink and downlink coherence; η_{ant} denotes the overall efficiency of each element in the array, which is squared because it affects the system both during transmission and reception; and η_{ddm} is an efficiency related to processing the received samples into a DDM. For the purposes of this section, we assume that $\eta_{arr} = 0.93$, $\eta_{ant} = 0.70$, and $\eta_{ddm} = 1$. The first two values are obtained from performance data in the DSN, while the last value is used for simplicity's sake.

B. Cost Model

The life-cycle cost (LCC) of a planetary radar system can be broadly divided into two categories: an initial nonrecurring engineering cost for research and technology development (R&TD), and a recurring engineering cost to build the array and operate it over a certain time span. Here, we limit our attention to the recurring engineering costs and ignore any upfront R&TD costs. We also report all cost information normalized to facilitate relative comparison between different design choices and minimize any sensitivities related to costing information.[4]

1. Array Implementation Cost

The cost model for the planetary radar system makes the following assumptions:

- The cost of the array is the sum of the costs of individual array elements, plus an overhead for systems engineering and program management.

[4]The cost information contained in this document is of a budgetary and planning nature and is intended for informational purposes only. It does not constitute a commitment on the part of JPL and/or Caltech.

- The cost of shared systems in the array (e.g., time and frequency distribution, monitor and control software) is constant across all planetary radar architectures and thus can be neglected for relative costing purposes. This obviates the fact that larger arrays will require more area to place the antennas, thus driving up the cost of supporting equipment such as roads, trenches, and power and cable distribution.
- All antennas in the array are identical and thus benefit from economies of scale as the array grows.
- The cost associated with operations and maintenance are driven by the wear and tear of the mechanical antenna and the rate of replacement of the high-power amplifiers.
- The array construction costs are not affected by inflation (as if the entire array was built in one year), whereas the costs associated with maintenance and operation are always corrected by inflation. This correction factor is not shown in the article for simplicity's sake.

Using these assumptions, the total cost to implement the array is described by the parametric equation,

$$C_{\text{impl}} = (1 + \gamma_{\text{SE}}) \left(C_{\text{ant}} + C_{\text{hpa}} \right) \cdot N^{1-\gamma_n}, \tag{14}$$

where γ_{SE} is a factor to account for systems engineering and project management, C_{ant} denotes the cost of building one element in the array *excluding the high-power amplifier*, C_{hpa} is the cost of the high-power amplifier, and γ_n is a learning factor that models the economies of scale as the array grows in size.[5] We take $\gamma_{\text{SE}} = 0.15$ based on experience at JPL and assume somewhat pessimistically that $\gamma_n = 0.05$ based on [46].

The cost of one element in the array has been modeled parameterically as

$$C_{\text{ant}} = K_{\text{ref}} \left(\frac{f}{f_{\text{ref}}} \right)^{\alpha_1} \left(\frac{D}{D_{\text{ref}}} \right)^{\beta_1}, \tag{15}$$

where K_{ref} is the price of an individual antenna, f_{ref} is the notional (radio) frequency of operation, and D_{ref} is the diameter of an antenna. The exponents α_1 and β_1 indicate how the cost of the antenna scales with frequency and diameter. In order to calibrate the model parameters, we have used quotes from a 12-m, an 18-m, and a 34-m antenna and assume that they include all elements in the antenna except for the high-power amplifier (i.e., cost of foundation, pedestal, structure and panels of the reflector, receive electronics, and supporting equipment and services). Past studies have used similar scaling laws and shown, for instance, that β should be between 2.4 and 3 (e.g., [25]). Other authors (e.g., [23]) have approached the problem of

[5] As noted earlier, reduced implementation costs are possible if only a subset of the array elements is equipped with transmitters and sufficient Effective Isotropic Radiated Power (EIRP) is provided to satisfy the system requirements.

determining the cost of a large ground antenna using a bottoms-up approach rather than calibrated scaling laws.

For the cost of the high-power amplifier, we use a parametric equation that uses the cost of a known system together with basic scaling laws. In that sense, we follow [23] and assume that

$$C_{\text{hpa}} = \left(a + bP^{\beta_2}\right)\left(\frac{f}{f_{\text{ref}}}\right)^{\alpha_2}, \tag{16}$$

where a, b, α_2, and β_2 are parameters that are calibrated using a few rough order-of-magnitude estimates and past vendor quotes.

2. Array Operations and Maintenance

The costs associated with operations and maintenance are assumed to scale linearly with the number of elements in the array. For each element, the total maintenance cost is calculated as the sum of scheduled maintenance costs, plus unscheduled maintenance costs, plus an additional fixed cost to operate the array. For maintenance purposes, we utilize an industry study commissioned by the DSN to obtain estimates of the number of hours of scheduled maintenance per year, as well as the mean time between failures (MTBF) and mean time to repair (MTTR) for both the mechanical antenna and the high-power amplifiers. Using these inputs, the yearly operations and maintenance cost is estimated as

$$C_{o\&m} = N\left(C_{\text{sm}} + C_{um,ant} + C_{um,hpa}\right) + C_{fixed}, \tag{17}$$

where C_{sm} denotes the total yearly cost for scheduled maintenance for the mechanical antennas, including labor and parts; $C_{um,ant}$ denotes the cost of unscheduled maintenance of the mechanical antennas; $C_{um,hpa}$ captures the cost of replacing the high-power amplifiers whenever they fail; and C_{fixed} is calibrated to 7% of the array construction cost, and encompasses all operations costs and maintenance of electronics, infrastructures, and facilities. Finally, these yearly costs are discounted in time using an average inflation factor to obtain the present value of all operations and maintenance costs over a 10-year life span.

3. Cost Model Benchmark

In order to gain confidence in the results of the cost model, we collected information on the cost to build and operate the VLA.[6] The original cost estimate for the project was approximately \$75M in fiscal year 1975 (FY75) which, adjusted for inflation, is equivalent to \$360M (FY20). The VLA also underwent major upgrades starting in 2001, with an approximate cost of \$100M (FY20). Therefore, we estimate that rebuilding the VLA today would cost approximately \$450M (FY20). Further, in FY18

[6] Additional sanity checks were performed against cost information of a DSN 34-m antenna, but the results are not reported due to the sensitive nature of this information.

and FY19,[7] the National Science Foundation (NSF) awarded approximately $40M for the VLA operations and maintenance, which is equivalent to 9% of the construction cost.

Using the proposed cost model, we estimated the cost of building a receive-only array of 28 25-meter antennas with a maximum operating frequency of 50 GHz. Our model predicted a total construction cost of $475M (FY20), which results in an estimated relative error of 5.5%, approximately. Similarly, our model predicted a yearly operations and maintenance cost of $37M (FY20) (7.5% error), which is equivalent to 7.8% of the array implementation cost.

C. Siting

The cost model above does not include costs related to the site, in large part because there could be a number of programmatic considerations that would affect the choice of the site. There are, however, various technical considerations that could affect the performance of a radar array. We describe these here, listing them in no particular order.

- As we describe below, the optimum antenna diameter is in the range of 15 m to 18 m. As an illustrative value, we take the antennas to be arranged in a square configuration and separated by 50% of their diameter. This estimate is likely to be a lower limit on the amount of land required, but it suffices to provide the scale. As a specific example, an 100-antenna array, consisting of 18-m antennas, would require a site with dimensions of at least 240 m $\times$ 240 m, or approximately 0.06 km^2. Additional land would be needed for any buildings to house support equipment.

- Sites at lower latitudes provide access to a larger fraction of the sky. For a site at a geographical latitude b, a fraction of the sky $(1 + \cos b)/2$ is notionally available. Further, sites at higher geographical latitudes likely will require larger amounts of land, because the array would need to be extended in the north-south direction to mitigate the foreshortening that occurs for an array looking toward the southern sky (from a northern hemisphere site). In practice, a slightly smaller fraction of the sky likely will be accessible because antennas generally have elevation limits that do not allow them to point directly to the horizon.

- A site without significant topography (e.g., mountains) is desirable. Mountains or other topography could obstruct the view to the horizon, further reducing the fraction of the accessible sky. Further, there may be reflections of distant transmitters off mountains, which could reduce the signal-to-noise ratio of the return signal or obscure it altogether.

[7] We do not use the FY20 values because of concerns about possible effects of the COVID-19 pandemic.

- A remote site is desirable. While the planetary radar should operate in a spectral range allocated for radar (or radiolocation) purposes, a site too close to urban areas may suffer interference from unintentional out-of-band emissions from nearby transmitters. Further, considerations such as flight paths to nearby airports may restrict the directions to which the array could point or the times at which it could operate.

Presently, the cost model presented in Section IV.B does not explicitly account for cost escalation factors resulting from the array being built in a remote area. However, as a rough order of magnitude, the Department of Defense Facilities Pricing Guide assumes a $\sim$2.5$\times$ cost escalation factor for facilities built outside of the continental U.S. (e.g., Hawaii), while facilities built in remote sites within the U.S. (e.g., Goldstone, CA) have more moderate cost escalation values ($\sim$1$\times$ to $\sim$1.5$\times$).

V. Results

A. Baseline Performance

To compare the performance of the proposed array-based planetary radar system with current operational systems, we benchmark its asteroid detection capabilities with those of the AO and the GSSR. Figure 7 provides an estimate of the distance at which an asteroid is detectable as a function of its size. In particular, for cislunar asteroids (Figure 7, left panel), we have assumed the asteroid to be between 1 m and 1 km in diameter, with an average rotation period of 30 minutes. This matches the assumptions of [16], which are based on a comprehensive asteroid survey by [47]. On the other hand, to assess the performance of the system for asteroids in the main belt (between 2 AU and 4 AU, approximately), we have considered larger asteroids, from 10 km to 1000 km in diameter, and with a slower rotation period of 2 h. In all cases, we have assumed an albedo of 0.2, typical of S-group asteroids, while the assumed system parameters for the AO and the GSSR are provided in Table 1.

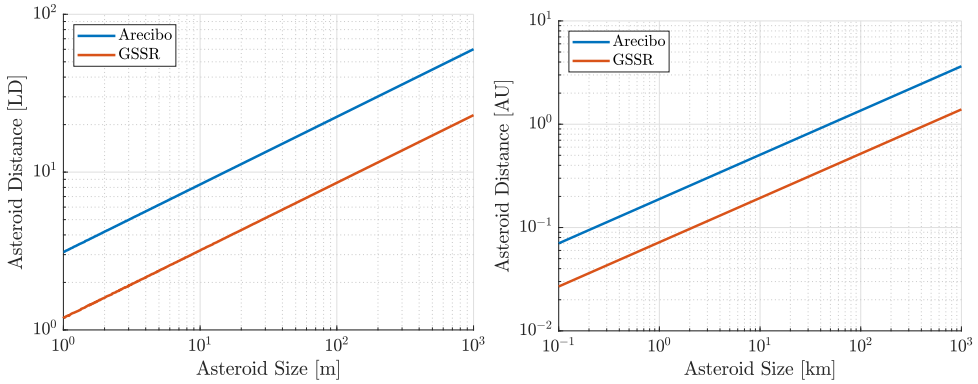

Figure 7. Performance of the AO and the GSSR. Left: Detectability of cislunar asteroids, for asteroid sizes ranging from 1 m to 1 km (1 lunar distance [LD] = 385,000 km). Right: Detectability of main-belt asteroids, for asteroid sizes ranging from 10 km to 1000 km.

Table 1. Radar System Parameters

	AO	GSSR	Units
Transmit frequency	2380	8560	MHz
Transmit power	900	450	kW
Aperture diameter	305	70	m
System temperature	23	18	K
Aperture efficiency	38	62	%
EIRP	19.76	10.98	TW

In Figure 7, the range at which an asteroid can be detected is linear with the asteroid size, when plotted in the logarithmic scale, as expected from Equation (11). To obtain the presented lines, we have assumed that the integration time Δt is equal to the round-trip light-time delay and that the switching time between transmit and receive modes is negligible. Note that the integration time might also be limited by other factors (e.g., rotation of asteroid to avoid "smearing" the measured DDMs, rotation of Earth), but we have obviated them here for simplicity's sake.[8]

Finally, under the assumptions previously presented, it is easy to show that the expected difference in performance between the AO and the GSSR can be expressed as analytically as

$$\left(\frac{R_{AO}}{R_{GSSR}}\right)^{3.5} = \left(\frac{f_{AO}}{f_{GSSR}}\right)^{1.5} \frac{P_{AO}}{P_{GSSR}} \left(\frac{\eta_{AO}}{\eta_{GSSR}}\right)^{2} \left(\frac{D_{AO}}{D_{GSSR}}\right)^{4} \frac{T_{GSSR}}{T_{AO}} \approx 32.8. \quad (18)$$

Therefore, the AO could detect the same asteroid up to 2.7 times farther from Earth than the GSSR.

B. Asteroid Detectability

1. Case Study 1: Cislunar Asteroid

We now consider the ability of the proposed array-based planetary radar system to detect and observe a cislunar asteroid. We assume the target has a reflectivity of 0.2, is 20 m in diameter, and rotates at a rate of one revolution every 30 minutes. To design the planetary radar system, we consider the following parameters:

- The transmit power available at each element of the array can be 20 kW, 30 kW, or 80 kW. These values are based on existing klystrons in operation at the DSN stations, as well as a JAXA-developed X-band SSPA. Note that additional

[8] Only 32% of the sky was accessible to Arecibo because the platform could obtain zenith angles limited to $\pm 20°$. The GSSR, on the other hand, has as much as 79% of the sky accessible and thus facilitates longer integration times.

development in SSPA technology is needed to achieve output powers close to 80 kW.

- The diameter of each element array can vary between 15 m, 18 m, 21 m, 25 m, and 34 m, based on a survey of ground antennas for similar observatories (Figure 8).

- The number of antennas in the array ranges from 1 to 200 based on current and proposed arrays (e.g., the ngVLA design requires up to 214 antennas).

- All antennas, regardless of diameter, are equipped with cryocooled receivers with an equivalent noise system temperature of 20 K at X-band. Also, the antenna illumination efficiency is set at 64%, based on experience from the DSN 34-m antennas.

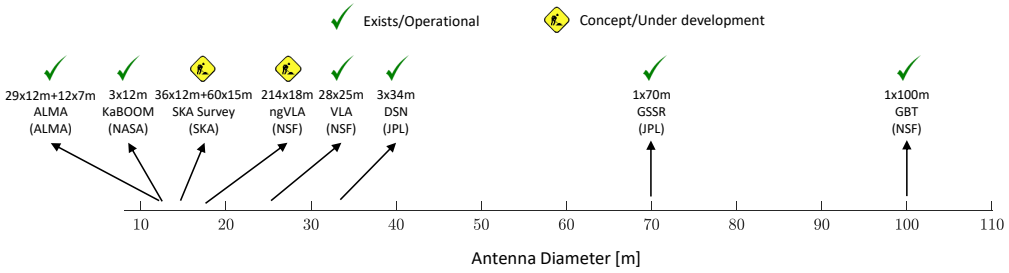

Figure 8. Sample of operational and conceptual antenna arrays. (ALMA is the Atacama Large Millimeter/submillimeter Array. KaBOOM is Ka-Band Objects Observation and Monitoring.)

Figure 9 shows the result of evaluating all possible combinations previously listed both in terms of performance (range at which a 20-m asteroid can be detected) and LCC (normalized with respect to the predicted cost for GSSR). Points highlighted in red represent the Pareto front of the tradespace, i.e., system designs that are optimal both in terms of performance and cost. The black dot represents the expected performance of the GSSR. As a first-order approximation, the relationship between asteroid-detectable range and LCC can be considered quasi-linear, especially as the number of antennas increases. Note also that not all evaluated architectures are represented in Figure 9. While the abscissa of Figure 9 is truncated at a LCC of 10× that of the GSSR, this quasi-linear scaling continues to larger values.

We examine the array configurations in the Pareto front (viz. Table 2). Results indicate that in all cases, the optimal transmit power occurs if each antenna is equipped with an 80-kW transmitter, hinting at the fact that provisioning transmit power using SSPAs is inexpensive compared to increasing system performance by building larger apertures or increasing the number of elements in the array. Similarly, an antenna size of 34 m is never selected, and instead, most architectures rely on 15-m or 18-m antennas. This is true up to a detection range of approximately 50 LD, which corresponds to an array of 200 18-m antennas.

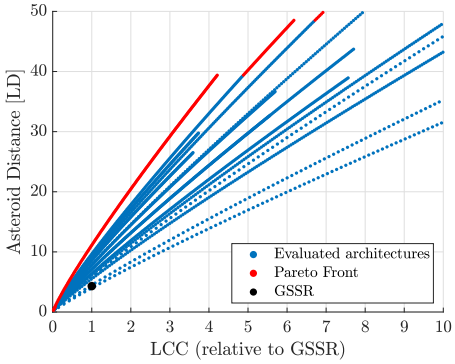

Figure 9. Detectability of a 20-m asteroid, shown in terms of the range normalized to the LD as a function of the radar array's LCC. The architectures shown illustrate the range of architectures explored, but not all are shown for clarity's sake. For reference, the performance of the GSSR is shown as well. (1 LD = 385,000 km)

Finally, we now consider how a planetary radar system based on an array of antennas could be designed to achieve a performance equivalent to the GSSR and Arecibo. For the GSSR, our model indicates that the optimal configuration requires 15 15-m antennas, which results in a system performance that is within 5% of that of the GSSR performance (while the LCC is estimated at only 33% of the GSSR). For Arecibo, the optimal configuration is an array of 46 15-m antennas.[9] Note that near-optimal configurations with an array of 18-m dishes are also possible, thus indicating that the cost of the system is not very sensitive to the exact antenna diameter. Therefore, the final architecture of the system might be driven by the availability of a given antenna type at the time of design and construction (e.g., the ngVLA is using more than 200 18-m antennas; therefore, it might be economically attractive to select that diameter to be able to leverage the R&TD investment in that type of antenna).

Table 2. Selected Array Configurations

Transmit Power (kW)	**Diameter** (m)	**No. of Elements** (-)	**Range** (normalized to AO)	**Range** (normalized to GSSR)	**Cost** (normalized to GSSR)
80	15	15	0.4	1.0	0.33
80	15	46	1.0	2.6	1.00
80	15	104	2.0	5.2	2.22
80	15	167	3.0	7.8	3.53
80	18	183	4.0	10.4	5.66
80	21	194	5.0	13.1	7.95

[9] We do not report the cost of the Arecibo Observatory because the cost models developed for this article are not applicable to a fixed reflector of 305 m in diameter.

2. Case Study 2: Main-Belt Asteroid

We now consider a second case study in which the planetary radar system is used to detect and observe asteroids in the main belt, which ranges approximately from 2 AU to 5 AU from Earth. As the average diameter of asteroids in this region varies significantly, we provide results for increasingly large asteroid sizes, from 1 km to 1000 km; the largest body in the asteroid belt, Ceres, has a diameter of 940 km, just under our maximum assumed size. We assume a typical rotation period of 2 h, which is a lower bound on rotation periods of main-belt asteroids [47] and thus a lower bound of performance of the system.

Figure 10 shows the Pareto-optimal architectures as a function of performance and cost. The tradespace has been color-coded according to the size of the asteroid, and the marker size has been set proportional to the number of antennas in the planetary radar array. The larger bodies of the main belt (Ceres, Vesta, Pallas, and Hygiea) are relatively easy to detect by arraying just a few 15-m antennas. The same is also true for bodies up to 100 km in diameter in the inner portions of the main belt, and these asteroids are relatively abundant in the survey by [47]. However, the number of antennas in the array must increase to as many as 160 to reach these objects in the outer portions of the main belt.

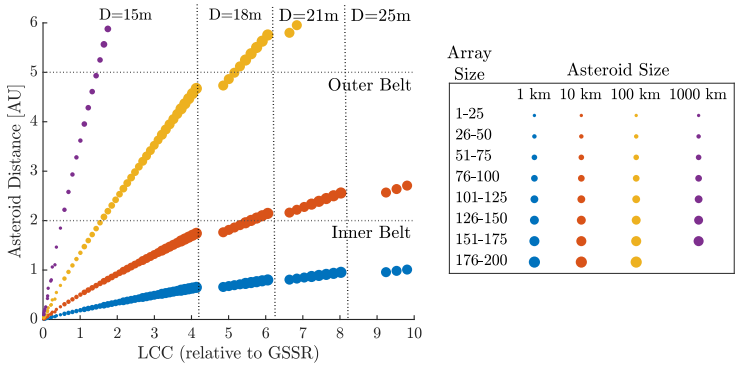

Figure 10. Asteroid Belt Detectability vs. Lifecycle Cost

Finally, detecting asteroids 10 km in diameter or smaller is quite challenging, even if larger antenna diameters are assumed. For instance, almost 200 18-m antennas are required to detect a 10-km asteroid at the closer edge of the inner asteroid belt, and similarly large arrays of 21-m antennas are required to reach beyond that point. For 1-km asteroids, detection at 2 AU is not possible even if 200 34-m antennas are used.

VI. Conclusions and Future Work

We have described the concept for a ground-based planetary radar array. The primary focus has been on a design ensuring that it could be used for scientific and planetary defense purposes with respect to near-Earth asteroids. However, such a radar array

would enable planetary science across the inner solar system and potentially well into the outer solar system. Further, such an array could be used for spacecraft tracking, particularly of uncooperative spacecraft, out at least to the orbit of the Moon for the purposes of safety and mission assurance.

The anticipated benefit of a radar array, consisting of multiple antennas operating coherently, is that it provides *graceful degradation*. Using the EIRP of the radar array as a metric for measuring performance, for a radar array of N antennas, its EIRP is proportional to N^2. Thus, if one of the antennas is out of operation, the radar array's performance is degraded by a factor of only $[(N-1)/N]^2$, which is marginal for a radar array consisting of even a moderate number of antennas. This graceful degradation is in contrast to the historical approach of utilizing a large, monolithic antenna equipped with a high-power transmitting system, in which any maintenance or component failure could remove it from service completely.

The system architecture (Figure 3) consists of four major subsystems. We describe each subsystem in turn, emphasizing that the components of the subsystems are at a high technology readiness, with many having been demonstrated either individually or collectively within NASA's DSN or within various radio astronomical arrays.

Using this architecture, a LCC model for a planetary radar array was developed (Section IV.B), which accounts for both the initial construction cost and operations for a specified duration. A number of different architectures were evaluated, with the Pareto front indicating that the optimal architecture would rely on antennas with diameters of approximately 15 m to 18 m, each equipped with transmitters of approximately 80 kW.

Acknowledgments

We would like to acknowledge the help of the different reviewers that contributed to this article, namely Mark Gatti, Leslie Deutsch, and Dimitri Antsos from the Jet Propulsion Laboratory.

References

[1] S. J. Ostro, *Encyclopedia of the Solar System*, 2nd ed. Elsevier, Inc., 2007, pp. 735–764.

[2] N. J. S. Stacy, D. B. Campbell, and P. G. Ford, "Arecibo radar mapping of the lunar poles: A search for ice deposits," *Science*, vol. 276, pp. 1527–1530, 1997.

[3] B. A. Campbell, D. B. Campbell, J. F. Chandler, A. A. Hine, M. C. Nolan, and P. J. Perillat, "Radar imaging of the lunar poles," *Nature*, vol. 426, pp. 137–138, Nov. 2003.

[4] M. A. Slade, B. J. Butler, and D. O. Muhleman, "Mercury radar imaging - Evidence for polar ice," *Science*, vol. 258, pp. 635–640, Oct. 1992.

[5] J. K. Harmon, M. A. Slade, R. A. Vélez, A. Crespo, M. J. Dryer, and J. M. Johnson, "Radar mapping of Mercury's polar anomalies," *Nature*, vol. 369, pp. 213–215, May 1994.

[6] D. O. Muhleman, B. J. Butler, A. W. Grossman, and M. A. Slade, "Radar images of Mars," *Science*, vol. 253, pp. 1508–1513, Sep. 1991.

[7] S. J. Ostro and G. H. Pettengill, "Icy craters on the Galilean satellites," *Icarus*, vol. 34, pp. 268–279, May 1978.

[8] D. O. Muhleman, A. W. Grossman, B. J. Butler, and M. A. Slade, "Radar reflectivity of Titan," *Science*, vol. 248, pp. 975–980, May 1990.

[9] Committee on the Planetary Decadal Survey, "Vision and Voyages for Planetary Science in the Decade 2013-2022," National Academy of Sciences, Report, 2011.

[10] S. R. Chesley, D. Farnocchia, M. C. Nolan, D. Vokrouhlický, P. W. Chodas, A. Milani, F. Spoto, B. Rozitis, L. A. M. Benner, W. F. Bottke, M. W. Busch, J. P. Emery, E. S. Howell, D. S. Lauretta, J.-L. Margot, and P. A. Taylor, "Orbit and bulk density of the OSIRIS-REx target Asteroid (101955) Bennu," *Icarus*, vol. 235, pp. 5–22, Jun. 2014.

[11] Committee to Review Near-Earth-Object Surveys, *Defending Planet Earth: Near-Earth-Object Surveys and Hazard Mitigation Strategies*. Washington, D.C.: National Academies Press, 2010.

[12] S. J. Ostro and J. D. Giorgini, "The role of radar in predicting and preventing asteroid and comet collisions with Earth," in *Mitigation of Hazardous Comets and Asteroids*, M. J. S. Belton, T. H. Morgan, N. H. Samarasinha, and D. K. Yeomans, Eds., 2004, p. 38.

[13] J. D. Giorgini, P. W. Chodas, M. A. Slade, R. A. Preston, and D. K. Yeomans, "DSN Radar Upgrade Study," Jet Propulsion Laboratory, National Aeronautics and Space Administration, Pasadena, CA, Tech. Rep., 2008. http://hdl.handle.net/2014/45704

[14] J. D. Giorgini, M. A. Slade, A. Silva, R. A. Preston, M. Brozovic, P. A. Taylor, and C. Magri, "Improved impact hazard assessment with existing radar sites and a new 70-m southern hemisphere radar installation," Jet Propulsion Laboratory, National Aeronautics and Space Administration, Pasadena, CA, Tech. Rep., 2009a. http://hdl.handle.net/2014/45220

[15] J. D. Giorgini, L. A. M. Benner, M. Brozović, M. W. Busch, D. B. Campbell, S. R. Chesley, P. W. Chodas, E. Howell, J.-L. Margot, A. Milani, P. Pravec, R. A. Preston, M.-E. Sansaturio, D. J. Scheeres, M. K. Shepard, A. Silva, M. A. Slade, P. A. Taylor, G. Valsecchi, D. Vokrouhlicky, and D. K. Yeomans, "Radar Astrometry of Small Bodies: Detection, Characterization, Trajectory Prediction, and Hazard Assessment," Jet Propulsion Laboratory, National Aeronautics and Space Administration, 2009, White Paper, submitted to the Planetary Sciences Decadal Survey (2013–2022). https://trs.jpl.nasa.gov/handle/2014/45703

[16] S. P. Naidu, L. A. Benner, J.-L. Margot, M. W. Busch, and P. A. Taylor, "Capabilities of earth-based radar facilities for near-earth asteroid observations," *The Astronomical Journal*, vol. 152, no. 4, p. 99, 2016.

[17] ESA, "SOHO spacecraft located with ground-based radar". https://soho.nascom.nasa.gov/newsroom/oldesapr/press27.html (accessed 2021)

[18] Jet Propulsion Laboratory, "New NASA Radar Technique Finds Lost Lunar Spacecraft," https://www.jpl.nasa.gov/news/new-nasa-radar-technique-finds-lost-lunar-spacecraft

[19] M. Brozović, R. S. Park, J. G. McMichael, J. D. Giorgini, M. A. Slade, D. S. Berry, J. S. Jao, F. D. Ghigo, P. A. Taylor, and E. Rivera-Valentín, "Radar Observations of

Spacecraft in Lunar Orbit," in *26th International Symposium on Space Flight Dynamics*, Jun. 2017.

[20] P. Vereš and S. R. Chesley, "High-fidelity Simulations of the Near-Earth Object Search Performance of the Large Synoptic Survey Telescope," *Astronomical Journal*, vol. 154, no. 1, p. 12, Jul. 2017.

[21] R. L. Jones, C. T. Slater, J. Moeyens, L. Allen, T. Axelrod, K. Cook, Ž. Ivezić, M. Jurić, J. Myers, and C. E. Petry, "The Large Synoptic Survey Telescope as a Near-Earth Object discovery machine," *Icarus*, vol. 303, pp. 181–202, Mar. 2018.

[22] R. Jedicke, B. T. Bolin, W. F. Bottke, M. Chyba, G. Fedorets, M. Granvik, L. Jones, and H. Urrutxua, "Earth's Minimoons: Opportunities for Science and Technology," *Frontiers in Astronomy and Space Sciences*, vol. 5, p. 13, 2018. https://www.frontiersin.org/article/10.3389/fspas.2018.00013

[23] J. Statman, D. Bagri, C. Yung, S. Weinreb, and B. MacNeal, "Optimizing the antenna size for the deep space network array," *The Interplanetary Network Progress Report*, Jet Propulsion Laboratory, Pasadena, CA, pp. 1–8, 2004. https://ipnpr.jpl.nasa.gov/progress_report/42-159/159B.pdf

[24] B. E. MacNeal and W. Hurd, "Parametric cost analysis of NASA's dsn array," in *SpaceOps 2004 Conference*, 2004, p. 433.

[25] J. Bunton, "Memo 90: Dish cost frequency scaling," Square Kilometer Array, Tech. Rep., 2007.

[26] R. Schilizzi, P. Alexander, and J. Cordes, "Memo 100: Preliminary specification for the square kilometre array," Square Kilometer Array, Tech. Rep., 2007.

[27] R. Selina, "System-level evaluation of aperture size," Next Generation Very Large Array, Tech. Rep., 2019.

[28] D. Jones, "Geometric configuration constraints for large deep space network arrays," *The Interplanetary Network Progress Report*, vol. 42, Jet Propulsion Laboratory, Pasadena, CA, no. 2004, p. 157, 2004. https://ipnpr.jpl.nasa.gov/progress_report/42-157/157F.pdf

[29] T. R. Hunter and P. J. Napier, "Antennas and Receivers in Radio Interferometry," in *Antennas and Receivers in Radio Interferometry*, Sep. 2016. https://arxiv.org/abs/1609.09376

[30] R. J. Selina, E. J. Murphy, M. McKinnon, A. Beasley, B. Butler, C. Carilli, B. Clark, S. Durand, A. Erickson, W. Grammer, R. Hiriart, J. Jackson, B. Kent, B. Mason, M. Morgan, O. Y. Ojeda, V. Rosero, W. Shillue, S. Sturgis, and D. Urbain, "The ngVLA Reference Design," in *Science with a Next Generation Very Large Array*, in Astronomical Society of the Pacific Conference Series, E. Murphy, Ed., vol. 517, Dec. 2018, p. 15.

[31] C Chang, *DSN Telecommunications Link Design Handbook*. Jet Propulsion Laboratory, California Institute of Technology, Pasadena, CA, 2021.

[32] V. Vilnrotter, P. Tsao, D. Lee, T. Cornish, J. Jao, and M. Slade, "Planetary radar imaging with the deep-space network's 34 meter uplink array," in *2011 IEEE Aerospace Conference*, 2011, pp. 1–13.

[33] V. Vilnrotter, D. Lee, T. Cornish, P. Tsao, L. Paal, and V. Jamnejad, "Uplink array concept demonstration with the EPOXI spacecraft," *IEEE Aerospace and Electronic Systems Magazine*, vol. 25, no. 5, pp. 29–35, May 2010.

[34] J. K. Harmon, "Planetary delay-doppler radar and the long-code method," *IEEE transactions on geoscience and remote sensing*, vol. 40, no. 9, pp. 1904–1916, 2002.

[35] N. Rodriguez-Alvarez, M. A. Slade, J. Jao, C. Lee, K. Oudrhiri, and J. T. Lazio, "Goldstone Solar System Radar (GSSR) Learning Manual," Jet Propulsion Laboratory, Tech. Rep., 2019. https://deepspace.jpl.nasa.gov/files/GSSR_learning_manual.pdf

[36] K. J. Quirk and M. Srinivasan, "GSSR Waveforms for Lunar Observations," *The Interplanetary Network Progress Report*, vol. 42-192, Jet Propulsion Laboratory, Pasadena, CA, pp. 1–46, Feb. 2013. https://ipnpr.jpl.nasa.gov/progress_report/42-192/192D.pdf

[37] V. Vilnrotter, D. Lee, P. Tsao, T. Cornish, and L. Paal, "Uplink array calibration via lunar doppler-delay imaging," in *2010 IEEE Aerospace Conference*, 2010, pp. 1–12.

[38] D. H. Rogstad, A. Mileant, and T. T. Pham, "Antenna arraying techniques in the deep space network," Jet Propulsion Laboratory, Tech. Rep., 2003.

[39] L. R. D'Addario, "Combining Loss of a Transmitting Array due to Phase Errors," *The Interplanetary Network Progress Report*, vol. 42-175, Jet Propulsion Laboratory, Pasadena, CA, pp. 1–7, Nov. 2008. https://ipnpr.jpl.nasa.gov/progress_report/42-175/175G.pdf

[40] L. D'Addario, R. Proctor, J. Trinh, E. Sigman, and C. Yamamoto, "Uplink Array Demonstration with Ground-Based Calibration," *The Interplanetary Network Progress Report*, vol. 42-176, Jet Propulsion Laboratory, Pasadena, CA, pp. 1–69, Feb. 2009. https://ipnpr.jpl.nasa.gov/progress_report/42-176/176D.pdf

[41] V. Vilnrotter, D. Lee, T. Cornish, P. Tsao, and L. Paal, "Uplink Arraying Experiment with the Mars Global Surveyor Spacecraft," *The Interplanetary Network Progress Report*, vol. 42-166, Jet Propulsion Laboratory, Pasadena, CA, pp. 1–14, Aug. 2006. https://ipnpr.jpl.nasa.gov/progress_report/42-166/166F.pdf

[42] L. D'Addario, R. Proctor, J. Trinh, E. Sigman, and C. Yamamoto, "Uplink Array Demonstration with Ground-Based Calibration," *The Interplanetary Network Progress Report*, vol. 42-176, Jet Propulsion Laboratory, Pasadena, CA, pp. 1–69, Feb. 2009. https://ipnpr.jpl.nasa.gov/progress_report/42-176/176D.pdf

[43] V. Vilnrotter, D. Lee, T. Cornish, P. Tsao, L. Paal, and V. Jamnejad, "Uplink array concept demonstration with the EPOXI spacecraft," in *2009 IEEE Aerospace Conference*, 2009, pp. 1–8.

[44] V. Vilnrotter, P. Tsao, D. Lee, T. Cornish, J. Jao, and M. Slade, "Planetary radar imaging with the Deep-Space Network's 34 meter Uplink Array," in *2011 Aerospace Conference*, 2011, pp. 1–13.

[45] S. J. Ostro, "Planetary radar astronomy," *Reviews of Modern Physics*, vol. 65, no. 4, p. 1235, 1993.

[46] W. J. Larson and J. R. Wertz, *Space Mission Analysis and Design*, 1992.

[47] P. Pravec, A. W. Harris, and T. Michalowski, "Asteroid rotations," *Asteroids III*, vol. 113, 2002.